TECHNICAL ARTICLE

Structural and thermoelectric properties of Pb$_4$In$_{2.6}$Bi$_{3.4}$Se$_{13}$

W. Wong-Ng [1,a)] J. Guo,[2] Y. Yan,[2] and J. A. Kaduk [3]

[1]*Materials Measurement Science Division, National Institute of Standards and Technology, Gaithersburg, Maryland 20899, USA*
[2]*State Key Laboratory of Advanced Technology for Materials Synthesis and Processing, Wuhan University of Technology, Wuhan, Hubei 430070, China*
[3]*Department of Biological and Chemical Sciences, Illinois Institute of Technology, Chicago, Illinois 60616, USA*

Quaternary selenide, Pb$_4$In$_{2.6}$Bi$_{3.4}$Se$_{13}$ ($x = 2.4$ member of the Pb$_4$(In$_x$Bi$_{6-x}$Se$_{13}$ solid solution), was synthesized by a solid-state technique, and its structure was determined using powder X-ray diffraction (XRD). Pb$_4$In$_{2.6}$Bi$_{3.4}$Se$_{13}$ crystallizes in the orthorhombic space group *Pbam* (No. 55) with $Z = 4$. Lattice parameters and calculated density were determined to be $a = 22.152(5)$ Å, $b = 27.454(5)$ Å, and $c = 4.1354(6)$ Å, $V = 2515.0(11)$ Å^3, and $D_x = 7.490$ g cm^{-3}. The structure consists of Z-shaped ribbon units and corner-shared infinite one-dimensional [InSe$_4$]$_\infty$ chains running parallel to the *c*-axis. The chains and ribbons are further connected by Pb atoms to form a three-dimensional network. Pb atoms are situated in the center of bicapped trigonal prisms. The compound exhibits a semiconductor feature. The Seebeck coefficient of Pb$_4$In$_{2.6}$Bi$_{3.4}$Se$_{13}$ was found to be -180 μV K^{-1} at 295 K and -380 μV K^{-1} at 600 K. Combining the values of Seebeck coefficient, electrical conductivity, and thermal conductivity yield a figure of merit, *ZT*, of about 0.175 at 700 K. The powder XRD pattern of Pb$_4$In$_{2.6}$Bi$_{3.4}$Se$_{13}$ was also determined. © *The Author(s), 2021. Published by Cambridge University Press on behalf of International Centre for Diffraction Data.* [doi:10.1017/S0885715621000385]

Key words: Pb$_4$In$_{2.6}$Bi$_{3.4}$Se$_{13}$, thermoelectric material, thermoelectric property measurements, crystal structure, powder X-ray diffraction pattern

I. INTRODUCTION

Materials that are capable of converting thermal energy into electricity and vice versa are known as thermoelectric materials. These materials can harvest thermal energy generated from natural heat sources (solar, geothermal, and human body) and from waste heat suppliers (industrial sector and motor vehicles). However, the relatively low efficiency of most of these materials has limited their widespread applications. Efficiency of the thermoelectric materials in general depends on the dimensionless figure-of-merit, *ZT*, which is defined as $ZT = \alpha^2\sigma/\kappa$, where T is the absolute temperature, α is the Seebeck coefficient or thermal power, σ is the electrical conductivity, and κ is the thermal conductivity ($\kappa = \kappa_e + \kappa_{ph}$) which is the sum of the contributions from the electronic component and the phonon component (Rowe, 1995). Therefore, a high Seebeck coefficient and high electrical conductivity combined with low thermal conductivity are necessary to achieve high *ZT*. However, due to the interdependence of these parameters, optimizing *ZT* is a formidable challenge. For example, since both electrons and phonons contribute to the thermal conductivity of a material, lowering the electrical contribution, κ_e, will reduce σ as well.

One of the most popular approaches to search for compounds with high *ZT* values is to search for semiconducting multi-component chalcogenides, followed by incorporating metal ions into the infinite metal-chalcogen frameworks (Kanatzidis *et al.*, 1996; Chung *et al.*, 2000; Choi *et al.*,

2001; Hsu *et al.*, 2004; Wang *et al.*, 2009). These ions act as rattlers in their local cavities, which create low-frequency vibration modes that scatter acoustic phonons and reduce the thermal conductivity. The most studied heavy-element materials include ternary and higher antimony chalcogenides (Takeuchi *et al.*, 1974; Nuffield, 1975; Matzat, 1979; Edenharter, 1980; Berlepsch *et al.*, 2001; Olsen *et al.*, 2007). For example, Pb$_4$Sb$_6$S$_{13}$ exhibits a complicated structure with large unit cells and a band gap that is expected to appear between fully occupied S *p*-states and the empty Pb and Sb *p*-states (Derakhshan *et al.*, 2006; Wang et al., 2009). According to these authors, replacing S atoms by Se atoms would shrink the band gap by elevating the occupied *p*-states. At the same time, the *ZT* value benefits from lowered phonon contribution to the thermal conductivity caused by the heavier chalcogen Se as compared to S.

In this report, we will discuss the synthesis, crystal structure, as well as temperature-dependent Seebeck coefficient, electrical conductivity, and thermal conductivity of the substituted ternary selenide Pb$_4$Sb$_6$Se$_{13}$ in which the Sb site is substituted by the mixed Bi/In site, resulting in a formula of Pb$_4$(In$_x$Bi$_{6-x}$)Se$_{13}$. The Seebeck coefficient and electrical conductivity of two members of Pb$_4$(In$_x$Bi$_{6-x}$)Se$_{13}$ ($x = 2.1$ and 2.8) have been studied at a relatively low temperature (up to 300 K) (Wang *et al.*, 2009). Furthermore, no thermal conductivity data and hence *ZT* values were available. In our work, the Seebeck coefficient and electrical conductivity measurements were performed for Pb$_4$In$_{2.6}$Bi$_{3.4}$Se$_{13}$ ($x = 2.6$ member) up to 700 °C. We also measured the temperature-dependent thermal conductivity so we were able to estimate the *ZT* value. The ICDD PDF database (Gates-Rector and Blanton,

---
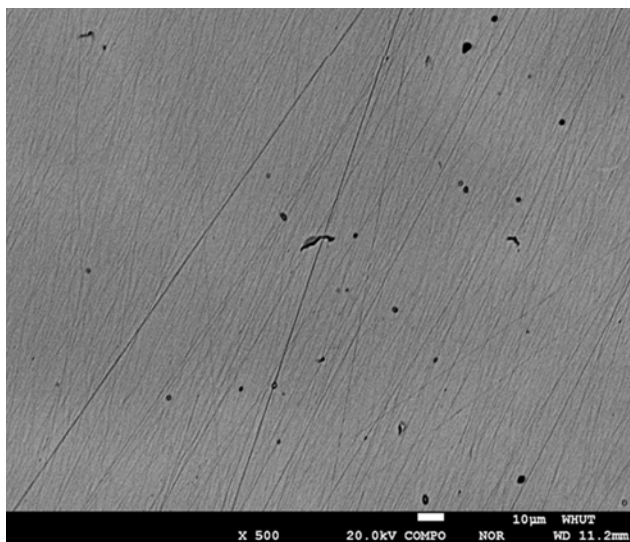
Figure 1. Backscattered electron image of a sample cut from $Pb_4In_{2.6}Bi_{3.4}Se_{13}$ showing the homogeneity of the sample.

2019) has the powder diffraction patterns for only the solid solution members $Pb_4In_{2.1}Bi_{3.9}Se_{13}$ and $Pb_4In_{2.8}Bi_{3.2}Se_{13}$. The powder X-ray diffraction (XRD) pattern for $Pb_4In_{2.6}Bi_{3.4}Se_{13}$ was, therefore, prepared and described in this report.

II. EXPERIMENTAL SECTION

A. Synthesis

To prepare $Pb_4In_{2.6}Bi_{3.4}Se_{13}$, stoichiometric quantities of high-purity elements (Pb/In/Bi/Se = 4:2.6:3.4:13) were first loaded into evacuated fused-silica tubes, followed by heat treatment from 300 to 1023 K; the latter temperature was maintained for 10 h before natural cooling to about 300 K. After subsequent melting, annealing (773 K, 48 h) and plasma activated sintering (PAS) treatments (763 K, 8 kN), we obtained the final dense ingot. The resulting ingot was ground into fine powders and examined on a PANalytical X'PERT PRO diffractometer (40 kV, 40 mA, 5–80° 2θ with a scanning rate of 10° min^{-1}) equipped with an X'celeator line detector and Cu radiation with λ of 1.54056 Å. (The purpose of identifying the equipment in this article is to specify the

experimental procedure. Such an identification does not imply recommendation or endorsement by the National Institute of Standards and Technology.) A backscattered electron (BSE) image of the resulting sample is shown in Figure 1, indicating a homogeneous sample.

B. X-ray Rietveld refinements and reference patterns

The $Pb_4In_{2.6}Bi_{3.4}Se_{13}$ phase was mounted as ethanol slurries on a zero-background cell. The XRD powder patterns of the former samples were measured on a Bruker D2 Phaser diffractometer (30 kV, 10 mA, 5–130° 2θ in 0.024° steps, 1 s step^{-1}) equipped with a LynxEye position-sensitive detector. Cu radiation with λ of 1.54056 Å.

The Rietveld refinement technique (Rietveld, 1969) with software suite GSAS II (Finger et al., 1994; Toby and von Dreele, 2013) was used to determine the structure of the $Pb_4In_{2.6}Bi_{3.4}Se_{13}$ phase. A reference pattern was obtained with a Rietveld pattern decomposition technique. Using this technique, the reported peak positions were derived from the extracted integrated intensities, and positions calculated from the lattice parameters. When peaks are not resolved at the resolution function, the intensities are summed, and an intensity-weighted d-spacing is reported.

C. Thermoelectric property measurements

The temperature-dependent electrical conductivity and Seebeck coefficient of samples were measured simultaneously using a commercial equipment (ZEM-3, UlvacRiko, Inc.) under 0.5 atm He atmosphere in the temperature range of 300–550 K. The thermal conductivity (κ) of the samples was calculated from the relationship $\kappa = DC_p d_e$, where D is the thermal diffusivity obtained by the laser flash method (LFA-457, Netzch, German), C_p is the specific heat measured by a differential scanning calorimeter (DSC Q20, TA Instrument, USA), and d_e is the density measured by the Archimedes method.

III. RESULTS AND DISCUSSION

Figure 2 shows the plots of Rietveld refinements for $Pb_4In_{2.6}Bi_{3.4}Se_{13}$, where observed (crosses), calculated (solid line), and difference XRD patterns (bottom) are shown. The

Figure 2. Rietveld refinement pattern for $Pb_4In_{2.6}Bi_{3.4}Se_{13}$, where observed (crosses, blue), calculated (solid line, Green), background (red), and difference XRD patterns (bottom) are shown. The tick marks indicate the calculated peak positions, and the difference pattern is plotted on the same scale as other patterns.
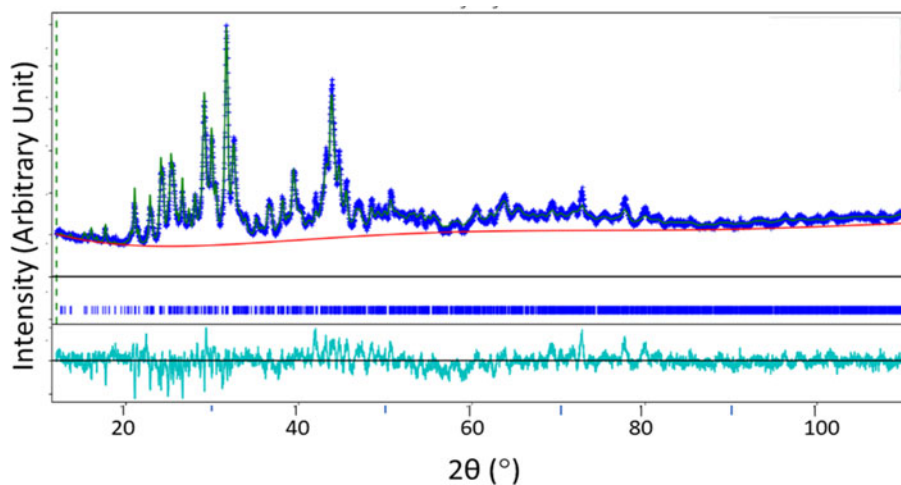
TABLE I. Refinement parameters for $Pb_4In_{2.6}Bi_{3.4}Se_{13}$.

Composition	$Pb_4In_{2.6}Bi_{3.4}Se_{13}$
R_p	0.04916
R_{wp}	0.06855
Refined # of parameters	72
Goodness of fit	2.556
Microstrain, "generalized" model parameters:	S400(1321.644), S040(139.951), S004(684224.77), S220(638.808), S202(25507.854), S002 (12976.743), G/L mix(1.00)
Background "Chebyschev" function:	1078(8), 203(14), −602(24), 4.8(4) × 10², 665(26), −5.6(4) × 10²

tick marks indicate the calculated peak positions, and the difference pattern is plotted on the same scale as other patterns. Table I gives various refinement R values and the goodness-of-fit value. The atomic coordinates and displacement parameters of $Pb_4In_{2.6}Bi_{3.4}Se_{13}$ are given in Table II (a total of 24 crystallographic inequivalent sites, 11 for cations and 13 for anions). Table III summarizes the selected bond distances concerning the mixed $(Bi/In)Se_6$ and $InSe_6$ distorted octahedra, $InSe_4$ tetrahedra, and $PbSe_8$ bicapped trigonal prisms.

A. Structure of Pb₄In₂.₆Bi₂.₄Se₁₃

$Pb_4In_{2.6}Bi_{3.4}Se_{13}$ (black color) crystallizes in the space group *Pbam* (No. 189), $Z = 4$. Lattice parameters and calculated density D_x are: $a = 22.152(5)$ Å, $b = 27.454(5)$ Å, and $c = 4.1354(6)$ Å, $V = 2515.0(11)$ Å³, and $D_x = 7.490$ g cm⁻³.

Since the atomic radius for Bi (1.60 Å) is greater than that of In (1.55 Å) (Slater, 1964; Shannon, 1976), one expects the unit cell volume of the members in the $Pb_4(In_xBi_{6-x}Se_{13})$ solid solution series to follow a trend as a function of x. The unit cell volume of $Pb_4In_{2.6}Bi_{3.4}Se_{13}$ (2515.0(11) Å³) was found to be

between that of $Pb_4In_{2.1}Bi_{3.9}Se_{13}$ (2535.8(9) Å³) and that of $Pb_4In_{2.8}Bi_{3.2}Se_{13}$ (2497.1(9) Å³) (Figure 3).

Figure 4 provides the crystal structure for $Pb_4In_{2.6}Bi_{3.4}Se_{13}$. The detailed crystal structure and electronic structure have been described by Wang *et al.* (2009). In summary, the complex structure features infinite chains of Z-shaped ribbon units (dark gray color) and tetrahedrons $[InSe_4]$ (green color) that share two vertices along the c-axis. The tetrahedral angles Se–In–Se in $[InSe_4]$ were found to be somewhat distorted from the ideal tetrahedral angles, namely: Se19–In17–Se19 of 107.4(16)°, In17–Se19–In17 of 107.4(16)°, and Se19–In17–Se30 of 116.3(13)°. The In–Se distances in these tetrahedra range from 2.53(5) to 2.70(6) Å, which are statistically in agreement with those found in compounds $Pb_4(In_xBi_{1-x}Se_{13})$ with $x = 2.0, 2.1$, and 2.8 (2.56–2.61 Å).

The Bi/In mixed sites (M) form both corner-shared and edged-sharing octahedra (Table III and Figure 4, M5, M7, M9, M11, M13, and M15). These octahedra form two groups of symmetry independent Z-shaped ribbons which run along the c-axis. One group consists of M5, M11, and M15, and the other one consists of M7, M9, and M13. Similar to $Pb_4In_{2.1}Bi_{3.9}Se_{13}$ and $Pb_4In_{2.8}Bi_{3.2}Se_{13}$, those distorted

TABLE II. Atomic coordinates for $Pb_4In_{2.6}Bi_{3.4}Se_{13}$.

Atom	x	y	z	Occ	Disp Para	Multiplicity
Pb1	0.6280 (8)	0.7512 (7)	0.50000	1.000	0.034 (3)	4
Pb2	0.1809 (7)	0.0704 (6)	0.50000	1.000	0.034 (3)	4
Pb3	0.1676 (8)	0.2255 (6)	0.50000	1.000	0.034 (3)	4
Pb4	0.4680 (9)	0.8491 (6)	0.50000	1.000	0.034 (3)	4
M5	0.8853 (8)	0.0850 (6)	0.50000	0.79/0.21	0.019 (3)	4
M7	0.6563 (8)	0.0242 (7)	0.50000	0.83/0.17	0.019 (3)	4
M9	0.6451 (8)	0.8907 (7)	0.00000	0.70/0.30	0.019 (3)	4
M11	0.0250 (10)	0.1560 (6)	0.00000	0.47/0.53	0.019 (3)	4
M13	0.50000	0.00000	0.00000	0.60/0.40	0.019 (3)	2
M15	0.00000	0.00000	0.00000	0.77/0.23	0.019 (3)	2
In17	0.7284 (12)	0.1607 (10)	0.00000	1.000	0.019 (3)	4
Se18	0.0258 (18)	0.2280 (13)	0.50000	1.000	0.018 (3)	4
Se19	0.7507 (20)	0.1084 (15)	0.50000	1.000	0.018 (3)	4
Se20	0.5585 (19)	0.8177 (16)	0.00000	1.000	0.018 (3)	4
Se21	0.8786 (18)	0.0112 (15)	0.00000	1.000	0.018 (3)	4
Se22	0.5847 (18)	0.0735 (15)	0.00000	1.000	0.018 (3)	4
Se23	0.5653 (18)	0.9457 (14)	0.50000	1.000	0.018 (3)	4
Se24	0.1447 (14)	0.1423 (14)	0.00000	1.000	0.018 (3)	4
Se25	0.3828 (20)	0.7993 (15)	0.00000	1.000	0.018 (3)	4
Se26	0.0144 (16)	0.0759 (15)	0.50000	1.000	0.018 (3)	4
Se27	0.7288 (20)	0.9786 (17)	0.00000	1.000	0.018 (3)	4
Se28	0.8953 (18)	0.1617 (16)	0.00000	1.000	0.018 (3)	4
Se29	0.7115 (15)	0.8458 (17)	0.50000	1.000	0.018 (3)	4
Se30	0.7279 (15)	0.7458 (13)	0.00000	1.000	0.018 (3)	4

"Disp Para" represents displacement parameter and "Occ" stands for occupancy. M5 stands for mixed site of (Bi5/In6); M7 stands for (Bi7/In8); M9 stands for (Bi9/In10); M11 stands for (Bi11/In12); M13 stands for (In13/Bi14); and M15 stands for (In15/Bi16).

TABLE III. Interatomic distances for $Pb_4In_{2.6}Bi_{3.4}Se_{13}$.

Contacts		Distance (Å)		Contacts		Distance (Å)	
Pb1	−Se20	3.16 (4)	×2	Pb1	−Se28	3.25 (3)	×2
Pb1	−Se29	3.19 (5)		Pb1	−Se30	3.03 (3)	×2
Pb1	−Se18	3.47 (5)		Pb2	−Se26	3.69 (4)	
Pb2	−Se21	3.32 (3)	×2	Pb2	−Se24	2.97 (3)	×2
Pb2	−Se27	3.18 (3)	×2	Pb2	−Se29	3.31 (5)	
Pb3	−Se18	3.14 (4)		Pb3	−Se24	3.12 (3)	×2
Pb3	−Se25	3.10 (3)	×2	Pb3	−Se29	3.32 (4)	
Pb3	−Se30	3.20 (2)	×2	Pb4	−Se18	3.33 (4)	
Pb4	−Se20	3.01 (4)	×2	Pb4	−Se22	3.19 (4)	×2
Pb4	−Se25	3.12 (4)	×2	Pb4	−Se23	3.42 (4)	
M5	−Se19	3.05 (4)		M5	−Se21	2.90 (3)	×2
M5	−Se26	2.87 (4)		M5	−Se28	2.96 (3)	×2
M7	−Se19	3.12 (5)		M7	−Se22	2.94 (3)	×2
M7	−Se23	2.95 (4)		M7	−Se27	2.90 (3)	×2
M9	−Se20	2.77 (5)		M9	−Se23	3.11 (3)	×2
M9	−Se27	3.04 (5)	×2	M9	−Se29	2.82 (2)	×2
M11	−Se18	2.86 (3)	×2	M11	−Se24	2.68 (3)	
M11	−Se26	3.03 (3)	×2	M11	−Se28	2.88 (4)	
M13	−Se22	2.76 (4)	×2	M13	−Se23	2.93 (3)	×4
M15	−Se21	2.71 (4)	×2	M15	−Se26	2.95 (3)	×4
In17	−Se19	2.57 (3)	×2	In17	−Se25	2.70 (6)	
In17	−Se30	2.53 (5)					

M5 stands for the mixed site of (Bi5/In6); M7 stands for (Bi7/In8); M9 stands for (Bi9/In10); M11 stands for (Bi11/In12); M13 stands for (In13/In14); M15 stands for (In15/Bi16).

octahedra (with Bi much greater than 50% occupancy in the Bi/In sites) were found to have three longer M–Se bonds vs. three shorter M–Se bonds, likely due to the presence of the $6s^2$ lone-pair electrons of the Bi^{3+} cations.

The four Pb sites (orange color in Figure 4) all have the bicapped trigonal prism coordination environment and they connect the $InSe_4$ tetrahedral units and the $(Bi/In)Se_6$ octahedral units to form a three-dimensional network. These Pb–Se distances have a wide range of values from 2.97(3) to 3.69(3) Å.

B. Thermoelectric properties

Figure 5 gives the electrical conductivity and Seebeck coefficient for $Pb_4In_{2.6}Bi_{3.4}Se_{13}$ as a function of temperature ($f(T)$), and Figure 6 shows the thermal conductivity and ZT for $Pb_4In_{2.6}Bi_{3.4}Se_{13}$ as $f(T)$. The negative value of α implies the materials to be n-type semiconductors. It is seen that as

Figure 4. Crystal structure of $Pb_4In_{2.6}Bi_{3.4}Se_{13}$ showing Z-shaped ribbons (M5 stands for Bi5/In6, M7 stands for Bi7/In8, M9 stands for Bi9/In10, M11 stands for Bi11/In12, M13 stands for Bi13/In14, and M15 stands for Bi15/In16). Pb atoms are shown as orange spheres and the $[InSe_4]_\infty$ tetrahedral chains (green).

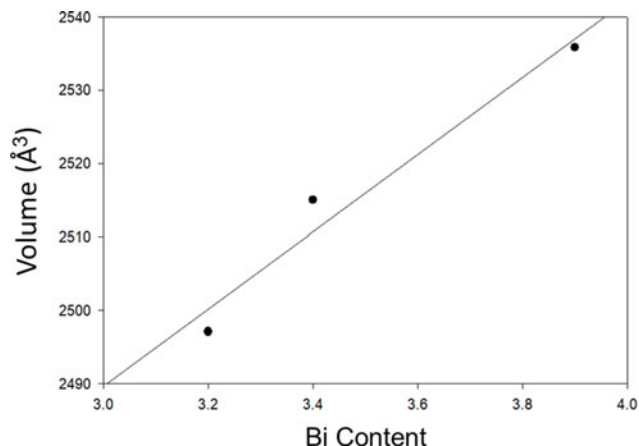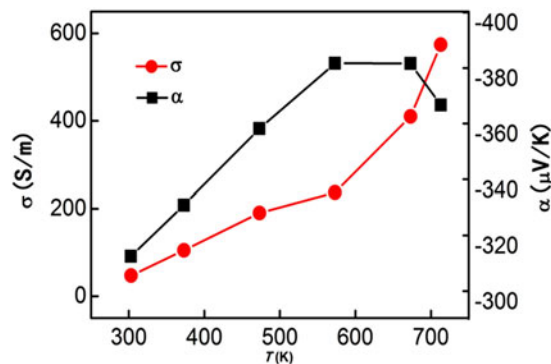Figure 5. Electrical conductivity and Seebeck coefficient for $Pb_4In_{2.6}Bi_{3.4}Se_{13}$ as $f(T)$.

Figure 3. Volume of $Pb_4(In_xBi_{6-x}Se_{13})$ solid solution vs. a function of (6-x) (or the Bi content).

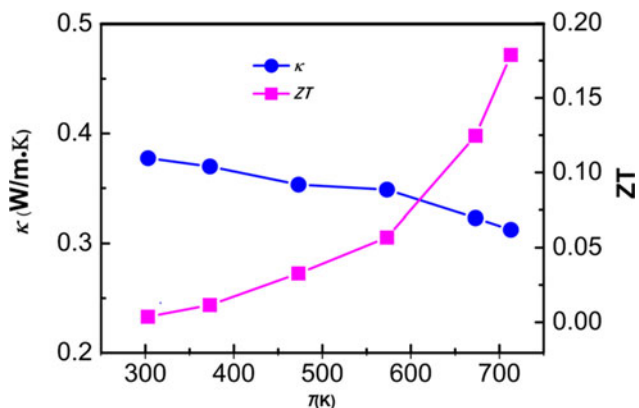Figure 6. Thermal conductivity and ZT for $Pb_4In_{2.6}Bi_{3.4}Se_{13}$ as $f(T)$.

TABLE IV. X-ray powder pattern for $Pb_4In_{2.6}Bi_{3.4}Se_{13}$, *Pbam* (No. 189), $a = 22.152(5)$ Å, $b = 27.454(5)$ Å, and $c = 4.1354(6)$ Å, $V = 2515.0(11)$ Å^3, $D_x = 7.49$ g cm^{-3}.

d	2θ	I	h	k	l	d	2θ	I	h	k	l
7.1307	12.40	10	3	1	0	7.0549	12.54	16	2	3	0
6.8634	12.89	5	0	4	0	6.5030	13.61	20	3	2	0
5.8342	15.17	24	2	4	0	5.7467	15.41	17	3	3	0
5.5381	15.99	59	4	0	0	5.4288	16.31	7	4	1	0
5.3295	16.62	21	1	5	0	5.0272	17.63	102	3	4	0
4.7380	18.71	20	4	3	0	4.5756	19.38	1	0	6	0
4.4810	19.80	3	1	6	0	4.4061	20.14	12	3	5	0
4.3739	20.29	4	5	1	0	4.3100	20.59	65	4	4	0
4.2290	20.99	164	2	6	0	4.2163	21.05	133	5	2	**0**
4.1354	21.47	64	0	0	1	3.9596	22.44	6	0	2	1
3.8992	22.79	240	4	5	0	3.8894	22.85	29	3	6	0
3.8742	22.94	21	2	0	1	3.8619	23.01	65	1	7	0
3.8362	23.17	2	2	1	1	3.7286	23.85	61	2	2	1
3.7223	23.89	22	5	4	0	3.7151	23.93	10	1	3	1
3.6970	24.05	188	2	7	0	3.6921	24.08	162	6	0	0
3.6591	24.30	345	6	1	0	3.5774	24.87	111	3	1	1
3.5677	24.94	21	2	3	1	3.5654	24.95	15	6	2	0
3.5421	25.12	54	0	4	1	3.5274	25.23	398	4	6	0
3.4977	25.44	168	1	4	1	3.4896	25.51	185	3	2	1
3.4637	25.70	90	3	7	0	3.4480	25.82	3	5	5	0
3.4317	25.94	43	0	8	0	3.4239	26.00	60	6	3	0
3.3913	26.26	47	1	8	0	3.3738	26.40	18	2	4	1
3.3566	26.53	343	3	3	1	3.3136	26.88	57	4	0	1
3.2897	27.08	20	4	1	1	3.2780	27.18	14	2	8	0
3.2672	27.27	127	1	5	1	3.2515	27.41	64	6	4	0
3.2210	27.67	2	4	2	1	3.2007	27.85	46	4	7	0
3.1937	27.91	80	3	4	1	3.1829	28.01	225	5	6	0
3.1655	28.17	1	2	5	1	3.1438	28.37	51	7	1	0
3.1156	28.63	131	4	3	1	3.1121	28.66	2	3	8	0
3.0837	28.93	409	7	2	0	3.0680	29.08	723	0	6	1
3.0638	29.12	2	6	5	0	3.0390	29.37	190	1	6	1
3.0219	29.54	5	1	9	0	3.0154	29.60	151	3	5	1
2.9909	29.85	54	7	3	0	2.9840	29.92	727	4	4	1
2.9567	30.20	33	2	6	1	2.9409	30.37	1	2	9	0
2.9367	30.41	326	5	7	0	2.8739	31.09	2	7	4	0
2.8705	31.13	85	5	3	1	2.8370	31.51	670	4	5	1
2.8332	31.55	116	3	6	1	2.8225	31.67	999	1	7	1
2.8193	31.71	9	3	9	0	2.7691	32.30	138	8	0	0
2.7666	32.33	211	5	4	1	2.7562	32.46	47	2	7	1
2.7551	32.47	239	8	1	0	2.7542	32.48	149	6	0	1
2.7454	32.59	39	0	10	0	2.7418	32.63	10	7	5	0
2.7404	32.65	174	6	1	1	2.7245	32.85	8	1	10	0
2.7131	32.99	82	5	8	0	2.7003	33.15	58	6	2	1
2.6883	33.30	92	6	7	0	2.6837	33.36	8	4	6	1
2.6719	33.51	24	4	9	0	2.6554	33.73	88	3	7	1
2.6483	33.82	34	5	5	1	2.6409	33.92	15	0	8	1
2.6373	33.96	62	6	3	1	2.6223	34.17	10	1	8	1
2.6028	34.43	34	7	6	0	2.5733	34.84	7	3	10	0
2.5679	34.91	6	8	4	0	2.5560	35.08	186	6	4	1
2.5311	35.44	20	4	7	1	2.5223	35.56	8	5	6	1
2.5136	35.69	55	6	8	0	2.5125	35.71	3	5	9	0
2.5027	35.85	14	7	1	1	2.4866	36.09	26	3	8	1
2.4724	36.31	4	8	5	0	2.4721	36.31	8	7	2	1
2.4629	36.45	2	7	7	0	2.4618	36.47	216	6	5	1
2.4597	36.50	29	4	10	0	2.4516	36.63	37	9	1	0
2.4399	36.81	150	1	9	1	2.4348	36.89	1	2	11	0
2.4235	37.07	11	7	3	1	2.3967	37.50	19	2	9	1
2.3944	37.53	21	5	7	1	2.3837	37.71	26	4	8	1
2.3769	37.82	20	9	3	0	2.3690	37.95	2	8	6	0
2.3644	38.03	5	3	11	0	2.3600	38.10	302	7	4	1
2.3597	38.11	21	6	6	1	2.3337	38.55	1	5	10	0
2.3295	38.62	2	3	9	1	2.3264	38.67	125	7	8	0
2.3169	38.84	3	9	4	0	2.3009	39.12	69	8	0	1
2.2928	39.26	182	8	1	1	2.2878	39.35	154	0	12	0
2.2872	39.36	63	0	10	1	2.2852	39.40	101	7	5	1

Continued

TABLE IV. Continued

d	2θ	I	h	k	l	d	2θ	I	h	k	l
2.2757	39.57	56	1	12	0	2.2754	39.57	2	4	11	0
2.2752	39.58	78	1	10	1	2.2692	39.69	62	8	2	1
2.2621	39.82	32	8	7	0	2.2539	39.97	107	6	7	1
2.2460	40.11	18	9	5	0	2.2442	40.15	12	4	9	1
2.2405	40.22	18	2	12	0	2.2400	40.23	71	2	10	1
2.2314	40.39	91	8	3	1	2.2152	40.70	13	10	0	0
2.2081	40.83	5	10	1	0	2.2028	40.94	39	7	6	1
2.1962	41.06	65	7	9	0	2.1870	41.25	14	10	2	0
2.1848	41.29	44	3	10	1	2.1816	41.35	11	8	4	1
2.1745	41.49	18	5	11	0	2.1677	41.63	13	9	6	0
2.1550	41.89	197	8	8	0	2.1480	42.03	77	6	8	1
2.1473	42.05	6	5	9	1	2.1269	42.47	78	1	11	1
2.1221	42.57	27	8	5	1	2.1160	42.70	148	7	7	1
2.1145	42.73	8	4	12	0	2.1140	42.74	29	4	10	1
2.1088	42.85	40	9	1	1	2.1082	42.86	2	10	4	0
2.1023	42.99	112	1	13	0	2.0981	43.08	161	2	11	1
2.0904	43.24	412	9	2	1	2.0848	43.37	4	9	7	0
2.0745	43.59	98	2	13	0	2.0738	43.61	46	7	10	0
2.0677	43.74	941	0	0	2	2.0677	43.74	112	6	11	0
2.0608	43.90	43	9	3	1	2.0556	44.01	170	8	6	1
2.0544	44.04	287	10	5	0	2.0526	44.08	2	3	11	1
2.0503	44.14	103	8	9	0	2.0442	44.27	14	6	9	1
2.0360	44.46	1	1	2	2	2.0328	44.54	53	5	12	0
2.0324	44.54	4	5	10	1	2.0304	44.59	63	3	13	0
2.0276	44.66	514	7	8	1	2.0213	44.80	20	9	4	1
2.0085	45.10	63	11	1	0	2.0001	45.30	14	9	8	0
1.9938	45.46	321	1	12	1	1.9936	45.46	14	4	11	1
1.9925	45.49	19	11	2	0	1.9846	45.68	1	8	7	1
1.9843	45.69	1	2	3	2	1.9737	45.94	5	9	5	1
1.9732	45.96	1	4	13	0	1.9705	46.02	1	3	2	2
1.9700	46.04	4	2	12	1	1.9668	46.11	19	11	3	0
1.9610	46.26	13	0	14	0	1.9597	46.29	1	7	11	0
1.9533	46.45	10	1	14	0	1.9527	46.47	7	10	0	1
1.9496	46.55	19	8	10	0	1.9489	46.56	4	2	4	2
1.9478	46.59	110	10	1	1	1.9456	46.65	2	3	3	2
1.9444	46.68	70	6	10	1	1.9397	46.80	54	7	9	1
1.9371	46.86	10	4	0	2	1.9333	46.96	9	10	2	1
1.9324	46.98	3	11	4	0	1.9321	46.99	15	3	12	1
1.9310	47.02	49	2	14	0	1.9288	47.08	83	10	7	0
1.9277	47.11	4	1	5	2	1.9247	47.18	13	5	11	1
1.9199	47.31	56	9	6	1	1.9156	47.42	1	9	9	0
1.9123	47.51	17	3	4	2	1.9111	47.54	1	8	8	1
1.9097	47.58	9	10	3	1	1.8953	47.96	16	3	14	0
1.8951	47.97	1	4	3	2	1.8827	48.30	146	4	12	1
1.8782	48.43	161	10	4	1	1.8740	48.54	5	1	13	1
1.8719	48.60	2	3	5	2	1.8643	48.81	11	4	4	2
1.8616	48.88	3	9	7	1	1.8612	48.90	25	10	8	0
1.8576	49.00	38	2	6	2	1.8565	49.03	26	5	2	2
1.8541	49.09	7	2	13	1M	1.8541	49.09	27	7	12	0M
1.8539	49.10	28	8	11	0	1.8494	49.23	49	6	11	1
1.8485	49.25	20	4	14	0	1.8419	49.44	53	12	1	0
1.8398	49.50	1	10	5	1	1.8369	49.59	11	8	9	1
1.8331	49.70	18	6	13	0	1.8296	49.80	49	12	2	0
1.8268	49.88	57	4	5	2	1.8258	49.91	8	3	6	2
1.8243	49.95	23	5	12	1	1.8229	49.99	17	1	7	2
1.8226	50.00	32	3	13	1						

The particular peak that has the strongest intensity in the entire pattern is assigned an intensity of 999 and other lines are scaled relative to this value. The symbols "M" refers to peaks containing contributions from two reflections. The *d*-spacing values are calculated values from refined lattice parameters, and "I" represents integrated intensity values.

temperature increases, so are the Seebeck coefficients and electrical conductivity, further confirming the compound to be a semiconductor. There is a maximum of the Seebeck coefficient value at around 600 K, at the same time, the conductivity rapidly increases above 600 K, probably a result of the bipolar conduction effect (caused by the low carrier concentration). The bipolar effect (the band gap for $Pb_4In_3Bi_3Se_{13}$ was reported to be 0.6 eV (Wang et al., 2009)) is a negative process deteriorating the thermoelectric properties, particularly at high temperatures.

The structural and compositional complexity, the rattling effect of alkali metal and Pb^{2+} ions in the cavities, the alloy--type occupancy disorder among the In and Bi atoms in $Pb_4In_{2.6}Bi_{3.4}Se_{13}$ all combine to produce a low lattice thermal conductivity value. In Figure 6, one notes the κ values decrease as the temperature increases, ranging from 0.38 W m^{-1} K^{-1} down to 0.30 W m^{-1} K^{-1}, which is a relatively low value in the series of multinary chalcogenides.

The figure of merit (ZT) for the $Pb_4In_{2.6}Bi_{2.4}Se_{13}$ phase was estimated to be 0.175 at about 700 K. For comparison, ZT of pure Bi_2Te_3 is 0.5 and the optimized Bi_2Te_3 alloy is about 0.9 (an industrially used material). Although the Seebeck coefficient of $Pb_4In_{2.6}Bi_{3.4}Se_{13}$ is near that of Bi_2Te_3, the electrical conductivity is too small for practical thermoelectric applications. Therefore, a ZT of 0.175, while a respectable value, is rather low as compared to the 0.5–0.9 value of that of Bi_2Te_3, and $Pb_4In_{2.6}Bi_{3.4}Se_{13}$ is not likely a viable candidate for further optimization efforts.

C. Reference XRD pattern

The reference pattern of $Pb_4In_{2.6}Bi_{3.4}Se_{13}$ is provided in Table IV. As the compound has a large unit cell, one expects a great number of peaks in the XRD pattern. Therefore, we report the pattern to a limit of $2\theta < 50°$. In this pattern, the symbol "M" refers to peaks containing contributions from two reflections. The particular peak that has the strongest intensity in the entire pattern is assigned an intensity of 999 and other lines are scaled relative to this value. In general, the d-spacing values are calculated values from refined lattice parameters. The intensity values reported are integrated intensities (rather than peak heights) based on the corresponding profile parameters as reported in Table I. For resolved overlapped peaks, intensity-weighted calculated d-spacing, along with the observed integrated intensity and the hkl indices of both peaks (for "M") are used. For peaks that are not resolved at the instrumental resolution, the intensity-weighted average d-spacing and the summed integrated intensity value are used. In the case of a cluster, unconstrained profile fits often reveal the presence of multiple peaks, even when they are closer than the instrumental resolution. In this situation, both d-spacing and intensity values are reported independently.

IV. SUMMARY

Quaternary selenides, $Pb_4In_xM_{6-x}Se_{13}$ ($M = Bi$, $x = 2.6$), or $Pb_4In_{2.6}Bi_{3.4}Se_{13}$, was synthesized and characterized. The crystal structure, isostructural with that of $Pb_4In_2Bi_4S_{13}$, features a three-dimensional framework consisting of Z-shaped ribbon motifs and corner-sharing infinite one-dimensional $[InSe_4]$ chains running parallel to the c-axis, and connected with Pb atoms to form a three-dimensional network. For $Pb_4In_xM_{6-x}Se_{13}$, In and Bi atoms are distributed over sites M5–M15 with a varied ratio to form a solid solution. Measurements of electrical conductivity show increasing values with increasing temperature for $Pb_4In_xM_{6-x}Se_{13}$. The Seebeck coefficient of $Pb_4In_{2.6}Bi_{3.4}Se_{13}$ was found to be approximately -385 µV K^{-1} between 550 and 650 K, indicating the compound to be an n-type semiconductor. However, the conductivity increases with increasing temperature (Figure 5), indicating that In is not an effective dopant

in this system. Although the Seebeck coefficient of $Pb_4In_{2.6}Bi_{3.4}Se_{13}$ is near that of Bi_2Te_3, the electrical conductivity is too small (ZT of 0.175) for industrial thermoelectric applications. The results of transport data with a better dopant in future work may provide a clearer insight into the potential of this material system.

V. DEPOSITED DATA

The supplementary material for this article, which includes the Crystallographic Information Framework (CIF) file containing the results of the Rietveld refinement (including the raw data), was deposited with the ICDD. The data can be requested at info@icdd.com.

CONFLICTS OF INTEREST

The authors have no conflicts of interest to declare.

Berlepsch, P., Armbruster, T., Makovicky, E., Hejny, C., Topa, D., and Graeser, S. (**2001**). "The crystal structure of (001) twinned xilingolite, $Pb_3Bi_2S_6$," Can. Mineral. **39**, 1653–1663.

Choi, K. S., Chung, D.-Y., Mrotzek, A., Brazis, P., Kannewurf, C. R., Uher, C., Che, W., Hogan, T., and Kanatzidis, M. G. (**2001**). "Modular construction of $A_{1+x}M_{4-2x}M'_{7+x}Se_{15}$ (A=K, Rb; M=Pb,Sn; M'=Bi,Sb): a new class of solid state quaternary termoelectric compounds," Chem. Mater. **13**, 756–764.

Chung, D-Y, Hogan, T., Brazis, P., Rocci-Lane, M., Kannewurf, C., Bastea, M., Uher, C., and Kanatzidis, M. G. (**2000**). "$CsBi_4Te_6$: a high-performance thermoelectric material for low-temperature applications," Science **287**, 1024–1027.

Derakhshan, S., Asson, A., Taylor, N. J., and Kleinke, H. (**2006**). "Crystal and electronic structures and physical properties of two semiconductors $Pb_4Sb_6Se_{13}$ and $Pb_6Sb_6Se_{17}$," Intermetallics **14**, 198–207.

Edenharter, A. (**1980**). "Die Kristallstruktur von Heteromorphit, $Pb_7Sb_8S_{19}$," Z. Kristallogr. **151**, 193–202.

Finger, L. W., Cox, D. E., and Jephcoat, A. P. (**1994**). "A correction for powder diffraction peak symmetry due to axial divergence," J. Appl. Crystallogr. **27**, 892–900.

Gates-Rector, S. D. and Blanton, T. N. (**2019**). "The Powder Diffraction File: a quality materials characterization database," Powder Diffr. **34**, 352–360.

Hsu, K. F., Loo, S., Guo, F., Chen, W., Dyck, J. S., Uher, C., Hogan, T., Polychroniadis, E. K., and Kanatzidis, M. G. (**2004**). "Cubic $AgPb_mSbTe_{2+m}$: bulk thermoelectric materials with high figure of merit," Science **303**, 818–821.

Kanatzidis, M. G., McCarthy, T. J., Tanzer, T. A., Chen, L.-H., and Iordanidis, L. (**1996**). "Synthesis and thermoelectric properties of the new ternary bismuth sulfides $KBi_{6.33}S_{10}$ and $K_2Bi_8S_3$," Chem. Mater. **8**, 1465–1474.

Matzat, E. (**1979**). "Cannizzarite," Acta Crystallogr. B Struct. Sci. **35**, 133–136.

Nuffield, E. W. (**1975**). "The crystal structure of fülöppite, $Pb_3Sb_8S_{15}$," Acta Crystallogr. B Struct. Sci. **31**, 151–157.

Olsen, L. A., Balic-Zunic, T., Makovicky, E., Ullrich, A., and Miletich, R. (**2007**). "Hydrostatic compression of galenobismutite (PbBi$_2$S$_4$): elastic properties and high-pressure crystal chemistry," Phys. Chem. Miner. **34**(7), 467–475.

Rietveld, H. M. (**1969**). "A profile refinement method for nuclear and magnetic structures," J. Appl. Crystallogr. **2**, 65–71.

Rowe, D. M. (**1995**). *CRC Handbook of Thermoelectrics* (CRC Press, Boca Raton, FL).

Shannon, R. D. (**1976**). "Revised effective ionic radii and systematic studies of interatomic distances in halides and chalcogenides," Acta Crystallogr. A **32**, 751–767.

Slater, J. C. (**1964**). "Atomic radii in crystals," J. Chem. Phys. **41**, 3199. *Bibcode*: *1964JChPh..41.3199S*. doi:10.1063/1.1725697.

Takeuchi, Y., Takagi, J., and Yamanaka, T. (**1974**). "The crystal structure of PbS• 2Bi$_2$S$_3$," Proc. Japan Acad. **50**, 317–321.

Toby, B. H. and Von Dreele, R. B. (**2013**). "GSAS-II: the genesis of a modern open-source all purpose crystallography software package," J. Appl. Crystallogr. **46**(2), 544–549.

Wang, M. F., Huang, W. H., and Lee, C. S. (**2009**). "Synthesis and phase width of quaternary selendides Pb$_4$In$_x$Bi$_{6-x}$Se$_{13}$ (M=Bi, x=2.1–2.8; Sb, x=2)," Inorg. Chem. **48**, 6402–6408.